PAPER • OPEN ACCESS

Correlation of source parameters and beam properties in the early operation of the full size ITER negative ion beam source

To cite this article: M. Ugoletti *et al* 2024 *Nucl. Fusion* **64** 056035

OPEN ACCESS
IOP Publishing | International Atomic Energy Agency
Nuclear Fusion
Nucl. Fusion **64** (2024) 056035 (18pp)
https://doi.org/10.1088/1741-4326/ad383a

Correlation of source parameters and beam properties in the early operation of the full size ITER negative ion beam source

M. Ugoletti[1,2,*], **M. Agostini**[1,2], **C. Poggi**[1], **E. Sartori**[1,3], **G. Serianni**[1,2] and **B. Zaniol**[1]

[1] Consorzio RFX (CNR, ENEA, INFN, UNIPD, Acciaierie Venete SpA), Corso Stati Uniti 4, 35127 Padova, Italy
[2] ISTP-CNR, Institute for Plasma Science and Technology, corso Stati Uniti 4, 35127 Padova, Italy
[3] Università degli Studi di Padova, via VIII Febbraio 2, 35122 Padova, Italy

E-mail: margherita.ugoletti@igi.cnr.it

Received 10 August 2023, revised 6 February 2024
Accepted for publication 27 March 2024
Published 10 April 2024

Abstract

One of the requirements of Heating and current drive Neutral Beam injectors for ITER is a beam homogeneity greater than 90%, to achieve an optimal beam transmission while keeping the heat load consistently low on the acceleration electrodes. The large size and complexity of ITER negative ion source play a key role in determining the homogeneity of the negative ion current of each of the 1280 beamlets and their divergence, and it is studied in the full-scale prototype source SPIDER. In this work the plasma properties are studied by spectroscopic and electrostatic measurements in the drivers, where the plasma is generated, and in the expansion region, where the plasma drifts and negative ions are produced, and they are correlated with the properties of the beam. The non-homogeneous plasma density profile is related to the non-homogeneous availability of negative ions along the beam vertical profile, with and without cesium evaporation. Visible tomography, a technique capable of characterizing isolated beamlet properties, is used to study the beam's dependence on plasma uniformity along the entire beam profile. Using these tools, it has been demonstrated how an increase in plasma density is linked to an improvement in beam homogeneity. The latter has been directly correlated with plasma homogeneity. The magnetic filter field and biases of the plasma grid and bias plate are responsible for the variation in plasma density and its homogeneity. Non-uniformities in the plasma's top/bottom and left/right distributions have been studied and partially addressed experimentally. The first issue was resolved by adjusting the radio-frequency power supplied to the plasma in different vertical regions, while the second issue was addressed by reversing the direction of the magnetic filter field and increasing the plasma density.

* Author to whom any correspondence should be addressed.

Keywords: neutral beam injection, negative ion source, negative ion beam

(Some figures may appear in colour only in the online journal)

1. Introduction

To satisfy the requirements for ITER Heating Neutral Beam (HNB), several beam properties must be simultaneously achieved. SPIDER, the full-size prototype of the negative ion source for ITER HNB, has the goal of optimizing production and extraction of negative ions, in view of MITICA operation, the one-to-one prototype of the entire HNB for ITER. Among the various requirements to be satisfied, SPIDER aims to obtain the required negative ion current, electron-to-ion ratio and pulse duration, as well as the beam divergence and homogeneity needed. During summer 2021, SPIDER operation with cesium evaporation was performed for the first time. Despite several temporary technological limits, a first study of the source and beam performances during surface production was carried out, which is of major interest for the future HNB. Herein also the results of volume operation are described, as their knowledge proved important for the successful operation involving cesium.

To operate at the large current density and power required for ITER HNB, a beam homogeneity better than 90% is necessary, to avoid uneven heat load on the acceleration system, in particular by guaranteeing a uniform co-extracted electron current on the extraction grid, *i.e.* the grid through which negative ions are extracted and on which co-extracted electrons are deflected. Furthermore, low beam divergence is necessary to obtain an optimal transmission efficiency, reducing the heat loads on the Neutral Beam Injector (NBI) components, sputtering damages, and secondary emission currents.

This work presents the results achieved with the full size ITER negative ion source SPIDER in the early operation, both with and without cesium evaporation in the source. Spectroscopic and electrostatic measurements are used to study the plasma in the source, and they are correlated with the beam current, focusing on the role of the plasma density.

All lessons learned will be crucial for the operation of MITICA, the full-size prototype of ITER HNB.

A detailed description of SPIDER source and accelerator is in [1, 2]. A CAD rendering of the main components of the source is in figure 1. SPIDER beam is composed of 1280 beamlets, extracted through a total extraction area of 0.2 m^2 from the plasma generated in $1.9 \times 0.9\ m^2$ source. So far, SPIDER has only operated with a limited number of extracted beamlets (28/1280) [3], distributed across the entire vertical extent and one horizontal row of the beam, to perform initial beam homogeneity studies. To develop a comprehensive idea of the origin of the SPIDER beam non-homogeneity found experimentally [4], a characterization of the plasma in the source is necessary as discussed in [5]. Spectroscopic and electrostatic measurements allow to characterize the plasma from the eight Radio-Frequency (RF) drivers, where the plasma is produced, to the extraction region, where the negative ions are mostly produced and then extracted and accelerated by the acceleration system.

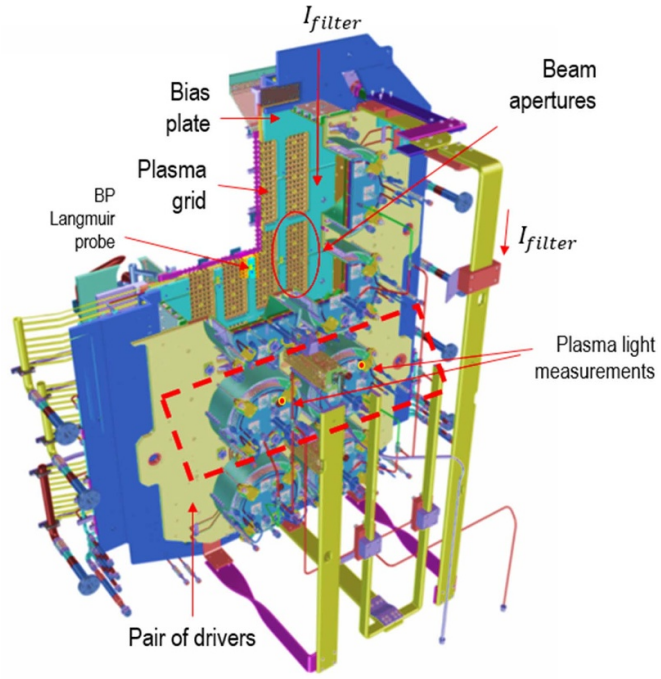

Figure 1. Detailed CAD rendering of SPIDER source.

The beam homogeneity is closely tied to the behavior of the source plasma, especially the uniformity of both negative (negative ions and electrons) and positive species at the extraction region. Ensuring uniformity of negative ions is crucial to achieve identical beamlet optics at all apertures, while a homogeneous electron density is essential to prevent localized heating of the extraction grid to which the co-extracted electrons are deflected. Diagnosing the plasma electronegativity $\alpha^- = \frac{n^-}{n_e}$ (where n^- represents the negative ion density and n_e the electron density) is not a trivial task. Since SPIDER operated with a limited number of extracted beamlets, the most accurate measurement of local n^- is provided by the beamlets themselves, given their isolation. Additionally, apart from assessing the local electronegativity, it is essential to study the uniformity of the plasma density distribution $(n = n^- + n_e = n^+)$, as it plays a crucial role in understanding the availability of negative ions along the entire beam source. Considering that future ITER negative ion NBIs are based on cesiated negative ion sources that produce negative ions through surface production, beam homogeneity is also dependent on a stable and effective cesium coverage on the Plasma Grid (PG) [6]. To reduce the likelihood of negative ion destruction and co-extracted electron current, a magnetic filter field is necessary to lower the electron temperature and density near the extraction region. The magnetic filter field in SPIDER

is generated using a combination of permanent magnets and the current flowing through the PG, from top to bottom in the standard direction (SFF), and from bottom to top in the reverse direction (RFF) [7]. The intensity of this field is on the order of mT (depending on the position in the source). Together with the magnetic filter field, the co-extracted electrons are further reduced by positively biasing the PG with respect to the source body, thus attracting more electrons electrostatically.

To enhance the effectiveness of the PG biasing, a dedicated Bias Plate (BP), consisting of a metallic plate that encloses the aperture groups, composed of five metallic plates, can be also biased.

One of the primary sources of plasma inhomogeneity can be attributed to the drift of ion-source plasma caused by the presence of the filter field and these biased surfaces, as already observed in SPIDER [8] and in other existing negative ion sources [9, 10]. Furthermore, the complexity of the source and the coupling between the drivers composing the source itself, can act as an additional factor contributing to plasma inhomogeneity, subsequently affecting the uniformity of the beam.

Taking into account all the aspects mentioned above, the HNB source is a complex system in which the properties of the plasma and the beam are intricately linked. To meet the requirements essential for future ITER HNB, optimization is needed across various aspects.

In this work, for the first time in a as much as possible comprehensive manner, the experimental results obtained with the SPIDER experiment, the first of its kind in terms of size for future ITER NBI systems, are presented. In particular, the behavior of both the plasma in the source and the beam when the key machine parameters are varied is investigated. Despite a substantial body of literature on the subject, from both experimental and numerical simulation perspectives, many of the experimental results found were not entirely predicted by simulations or machine design. In particular, the non-homogeneous effect of the magnetic filter field, in terms of strength and direction, on the plasma (and consequently, the beam) homogeneity inside the driver, both vertically and horizontally. Vertical non-homogeneities are linked to both plasma physics (e.g. drift) and the inherent structure of the source and magnetic filter components. Horizontal non-homogeneity, on the other hand, is discovered experimentally for the first time, and the two directions of the magnetic filter field are studied to determine the configuration which enables a more uniform plasma.

To study that, spectroscopy data are used as a primary tool to investigate the plasma in SPIDER source, aided and supported by Langmuir probe (LP) data, to provide a crucial interpretation of these widely available experimental measurements in this type of machine [11]. Spectroscopy is used as a tool to investigate plasma density inside the driver, demonstrating the linear correlation with the plasma light intensity and the plasma density, with dedicated measurements obtained from LPs. Since these probes were not available during the entire SPIDER's operation, this approach allowed for a more detailed study of plasma behavior in the source with high temporal and spatial resolution (spectroscopic measurements are available in each driver of the source).

Given the difficulties in diagnosing a large electronegative plasma, in the present SPIDER setup with reduced number of extracted beamlets, the beam diagnostics can provide a substantial contribution to the characterization of the plasma properties at the extraction region, and complement the spectroscopic and electrostatic measurements. The interpretation of such combined measurements, as presented in this paper, will provide key results for the understanding of the beam source behavior, fundamental for the future operation at full performance.

Starting from the analysis of the plasma emission - H_α - measured inside each driver, both the top–bottom and left–right plasma homogeneity is studied. The plasma vertical profile is then characterized in the expansion region, where the plasma produced inside each driver spreads and mixes. The spectroscopic measurements are compared with the electrostatic data collected by the set of LPs installed on the grids. These results are presented respectively in sections 2 and 3.

The properties of the plasma are then exploited to interpret the beam behavior, studied starting from the results obtained by the visible tomography, both without and with cesium evaporation, in sections 4 and 5 respectively.

2. Plasma in the drivers

In this section, the properties of the plasma within the drivers are examined using data from spectroscopic measurements. Optical emission spectroscopy is the main diagnostic of the plasma inside SPIDER, both in the drivers and extraction region. A comprehensive description of this diagnostic can be found in [12]. The light emitted by the plasma within the drivers, referred to as Plasma Light (with photon flux denoted as I_{PL}) is measured using 8 silicon photodiodes equipped with H_α filter, one for each driver. These photodiodes are installed in vacuum and positioned to directly observe the plasma light through dedicated openings on the back plate of each driver. They measure the integrated light emitted by the plasma near the driver axis. The time resolution of the photodiodes can reach 1 MHz, but they are usually used at 10–20 kHz. The data presented in this work are resampled at 0.1 s, averaging the plasma light measured in these intervals. At the typical electron temperature and density of the plasma in the driver – around 10 eV and 10^{18} m^{-3} [13] – the H_α emission is dominated by H excitations through direct electron collision. The I_{PL} in the drivers can thus be considered as representative of gas dissociation and plasma density [14, 15]. This relationship is experimentally demonstrated in figure 2, which shows the correlation between plasma light and electron density measured in SPIDER. These measurements were obtained using a set of movable Langmuir Probes (LP) installed on SPIDER during a dedicated experimental campaign [13]. These data were collected using only one RF generator at a time (i.e. one pair of drivers at a time), varying filter current, bias voltages, and RF power. Different colors represent various LPs, whose locations are indicated in the schematic on the right. Each of these probes measured inside a different driver. The voltage sweep of the probes was set to 1 Hz. The measurements presented

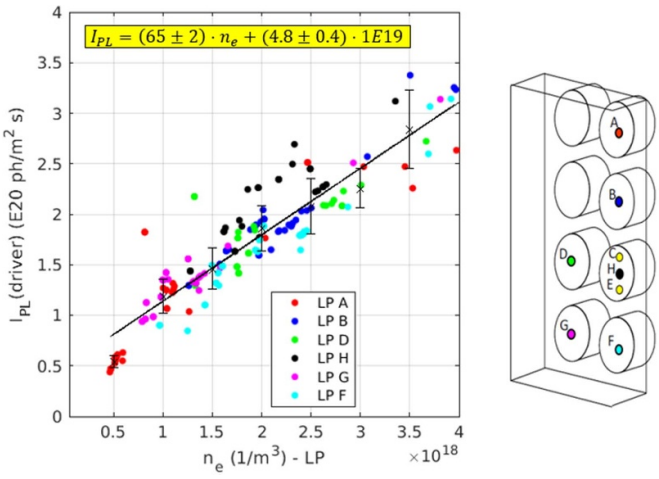

Figure 2. Dependence of the plasma light inside each driver on the electron density measured by Langmuir Probes inserted in the same driver. The position of each probe is shown in the schematic on the right. A linear fit is shown in black while the crosses with the error-bars represent the average value with its standard deviation of the plasma light for some values of electron density.

in figure 2 confirm that plasma light versus electron density measured by the LPs is approximately linear in a wide range of machine regimes. A linear fit of the plasma light as a function of electron density is shown in black in figure 2, with a correlation coefficient of 0.87. The points with $n_e < 1 \times 10^{18}$ m^{-3} do not enter in the fit as when the density is too low the linearity between the I_{PL} and n_e is not satisfied. The data presented in this work are taken at larger RF power with respect to the low-density measurements in figure 2. As an estimate of the dispersion of plasma light as a function of electron density, the mean and its standard deviation of certain plasma light values (sampled each 0.5×10^{18} m^{-3} electron density) are shown in figure 2. The average standard deviation is around 20%.

This confirms that plasma light can be used as an estimate of the plasma density inside the drivers throughout all the experimental campaigns, within the typical range of electron density and temperature in the SPIDER drivers.

Since the plasma density is higher in the drivers compared to the expansion region, it can be assumed that most of the plasma light collected along the line of sight is emitted within the drivers themselves.

Since the LP measurements in the driver were available for only a limited amount of experimental time (dedicated campaign), we utilize the relationship just demonstrated to study the dependence of plasma density inside the drivers on the source parameters, using only the measurement of plasma light.

The dependence of the total H_α plasma emission – the sum of the photon flux measured by the eight photodiodes – on the strength and direction of the magnetic filter field, for various values of the bias of PG and BP, is shown in figure 3. Each point represents the average photon flux resampled every 0.1 s. The bias applied to both grids, controlled in current, ranges from 0 to 140 A for the BP bias, I_{BP}, from 0 to 190 A for the PG bias, I_{PG}. It is important to note that the net current supplied to the grids differs from the nominal values due to a resistor of 0.6 Ω connected in parallel to each power supply. A slightly lower current is applied to the BP compared to the PG to prevent excessive heat load on the BP and because it was found to be the most effective operational condition. The summary of the applied current to the PG and BP is reported in table 1, along with the potential reached by the PG and BP with respect to the source body. For all bias current values, the potential reached by the PG and BP is higher in the standard configuration compared to the reversed configuration. Since grid potential variations are minimal and influenced by localized plasma characteristics, the measurements presented in this work are plotted as a function of the bias current to provide a clearer understanding of the dependence on these parameters of both the plasma in the drivers and in the expansion region (next section).

The filter field current is increased from 0.7 kA, which is the minimum current used during plasma initiation, to 2.5 kA, beyond which the plasma becomes unstable, considering the current operation with limited RF power (100 kW per generator out of the nominal 200 kW per generator). These data were collected with 4 × 100 kW of RF power per generator (50 kW per driver), in hydrogen operation without cesium evaporation and beam extraction. On the left side, the filter field is oriented in the standard direction (SFF), while on the right, the filter field is directed in the reverse direction (RFF). In both configurations, as the filter current increases, the plasma density in the RF drivers grows too. For all filter current values, except for the lowest bias in the RFF (represented by the blue markers in the right plot), plasma density is larger as bias increases. This is a well-known consequence of the presence of a magnetic filter field and biased surface in these types of plasma sources. In fact, the filter field concentrates the plasma within the drivers, while the presence of biased surfaces around the plasma, combined with the filter field, is helpful for plasma confinement and ultimately determines the achievable plasma density. These results have already been demonstrated both numerically [16, 17] and during dedicated experimental campaigns [9, 13, 18]. Measurements with LPs demonstrated that in SPIDER, the PG and BP bias modifies the plasma potential from the expansion region up to the drivers [13]. The increase in plasma density in the drivers when the PG and BP are biased can be roughly explained by the fact that this bias is positive relative to the source, reducing the difference of potential between the plasma in the driver and near the PG and BP.

The plasma density is slightly higher for all values of the filter field in the RFF compared to the SFF, as it can be noticed by comparing the total plasma light at intermediate filter current values, in the two configurations. The plasma light exhibits some fluctuations as the filter field is increased, which can be attributed to RF system-related issues, as described in detail in [19, 20].

However, the increase in the total plasma density with the PG and BP biases is more effective in the SFF.

Since one localized measurement is available for each driver, it is possible to investigate how PG and BP biases, as well as the direction and strength of the filter field, affect the

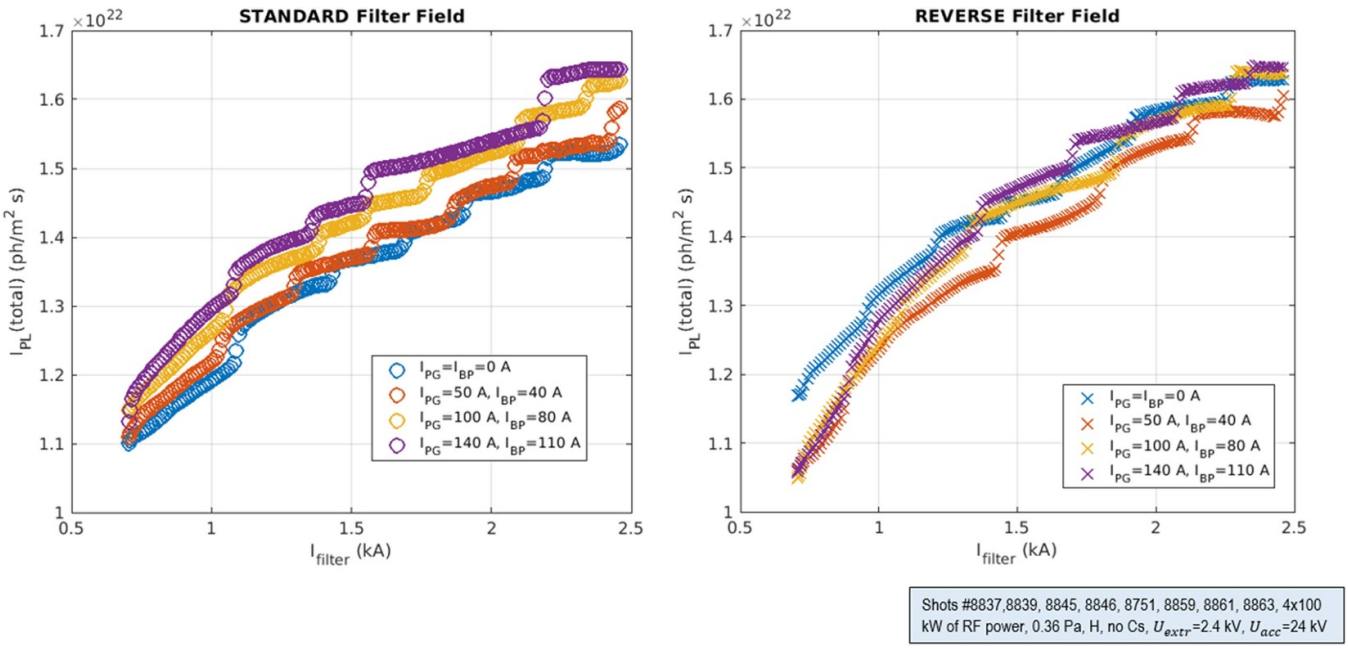

Figure 3. Total plasma emission as a function of the filter field current in the two configurations – SFF on the left, RFF on the right – for various values of total bias current.

Table 1. List of values of PG and BP bias currents and potentials in the experimental data presented in this section. The potentials are relative to the source body.

$I_{\mathrm{PG}}\,(A)$	$I_{\mathrm{BP}}\ (A)$	$V_{\mathrm{PG}}\ (\mathrm{V}) - SFF$	$V_{\mathrm{PG}}\ (\mathrm{V}) - RFF$	$V_{\mathrm{BP}}\ (\mathrm{V}) - SFF$	$V_{\mathrm{BP}}\ (\mathrm{V}) - RFF$
0	0	36	34	35	33
50	40	40	38	38	37
100	80	42	40	41	39
140	110	44	42	42	41

vertical profile of the plasma density. The evolution of the sum of plasma light measured in each horizontal pair of drivers is shown in figure 4. Only the two extreme cases of figure 3 are shown: $I_{\mathrm{PG}} = I_{\mathrm{BP}} = 0$ A on the left, $I_{\mathrm{PG}} = 140$ A, $I_{\mathrm{BP}} = 110$ A on the right. Different colors represent the 4 groups, or segments, that compose the SPIDER source, with one pair of drivers in each group (G1 at the top, G4 at the bottom of the source). The two line-styles indicate the direction of the filter field current. In these graphs, the segments highlighted are those at the top (G1, in black) and bottom (G4, in green) of the source, because they are the most influenced by changes in the filter field direction.

In the case with low biases (figure 4 - left), the plasma light increases with the filter field current everywhere except in the G4-SFF (green solid line) and G1-RFF (black dashed line). It can be observed that the behavior of these two pairs of drivers almost reverses when the filter field direction is inverted: the lowest I_{PL} is measured in the G4-SFF, and the largest one in G1-SFF; the opposite occurs in the reverse direction (lowest in G1-RFF for $I_{\mathrm{filter}} > 1.5$ kA, largest in G4-RFF, similar to G3). The two central groups, on the other hand, are less affected by the inversion of the magnetic field direction. In both configurations, their I_{PL} increases with the filter field current. The difference between the plasma densities in the same segment in the two configurations grows as the filter current increases (as indicated by the arrows in (figure 4 - left). These results reveal a top-bottom asymmetry in the plasma source, which reverses with the change in the filter field direction. This variation is greater than the uncertainty associated with using plasma light as an estimate of plasma density (see figure 2), so it can be concluded that this variation in plasma emission is a direct consequence of the local variation in plasma density. This means that the filter field enhances the plasma density inside the drivers, but the effect varies depending on their position and the direction of the filter field itself. This top-bottom non-uniformity, in both directions of the filter field, can be reduced biasing the BP and PG, as demonstrated in (figure 4 - right). It is evident that the presence of biased surfaces increases the plasma density in the drivers that have the lowest emission in the case with no bias. Indeed, the plasma light increases more significantly in G4-SFF and G1-RFF when biases are applied. As a result, there is an overall higher plasma density in both configurations, as previously observed in figure 3.

This top bottom non-uniformity can be somewhat expected, given that the filter field acts vertically. Any modification of the filter field and PG and BP biases affects the intensity and direction of the plasma drift in the expansion region [21]– as it will be discussed in detail in the next section. The

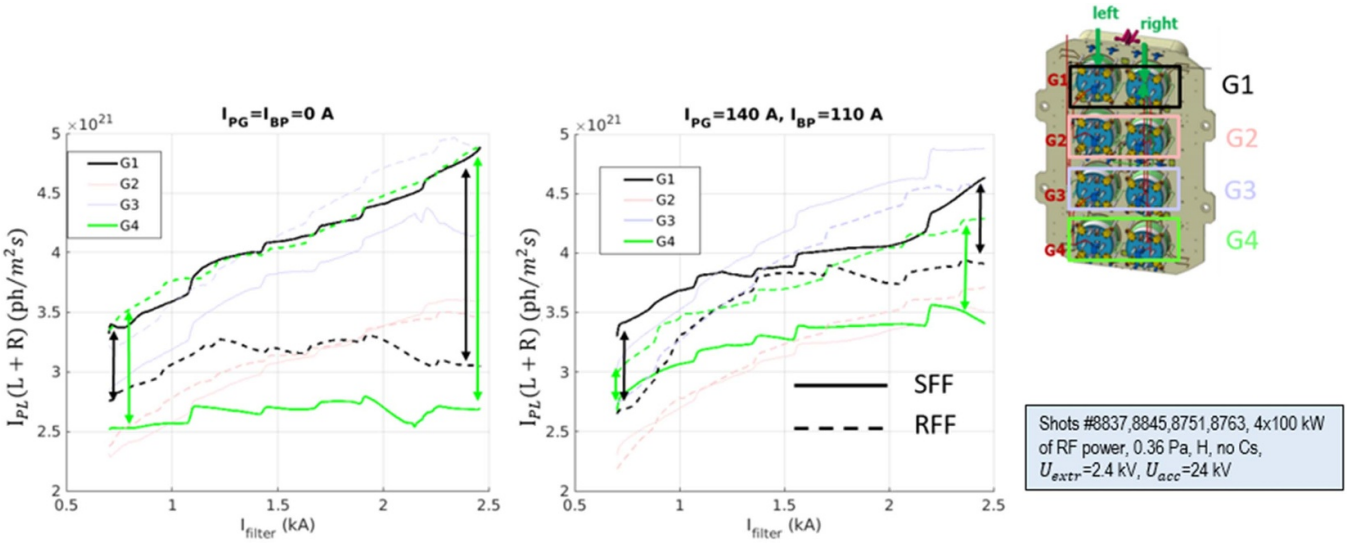

Figure 4. Sum of the plasma light measured in the 4 pairs of drivers (left + right) as a function of the filter field current for two values of BP and PG biases: $I_{PG} = I_{BP} = 0$A on the left, $I_{PG} = 140$A, $I_{BP} = 110$A on the right. The two line-styles represent the two configurations of filter field (solid lines SFF, dashed lines RFF). Arrows highlight the main changes in measured plasma light in top (black) and bottom (green) groups. On the right, a schematic of the drivers labeling is also shown.

plasma inside the drivers is partially influenced because the two regions are in contact. Furthermore, the inherent structure of the source, consisting of 4 vertically stacked RF generators, means that any difference in the coupling of one of these generators with the plasma, combined with the structure of the bus-bars that produce the filter field [7], may contribute to vertical non-uniformity. This partly explains why the top–bottom asymmetry is not completely reversed when the direction of the filter field is inverted.

Another piece of information can be derived by examining the filter field map within each driver, as depicted in figure 5(*a*) [22]. This map illustrates the magnetic field distribution in the pair of drivers located at the top of the source, with 3 kA of filter field current applied in both the standard direction (on the left) and the reverse direction (on the right). The magnetic filter field inside the pair of drivers is not perfectly symmetrical in the horizontal direction, and it depends on the direction of the current, as it is highlighted by the red arrows. The left-to-right asymmetry can be explained by considering the combined influence of the filter field current and the permanent magnets and ferromagnetic plate, which are also installed in the SPIDER plasma source to enhance plasma confinement and electron deflection [7]. In fact, the SPIDER filter field topology differs at the center and at the extremities of the source and depends on the applied filter current. Moreover, the filter field topology does not vary significantly at the center of the source as the filter current increases, while it significantly affects the extremities (in the vertical direction). This is evident when comparing the magnetic field lines within the drivers shown in figure 5(*a*): when the filter field is reversed, they exhibit greater symmetry compared to the standard direction configuration. Numerical simulations are currently in development, and initial results have recently been published in [23], where it is observed that the asymmetry of the filter field within driver pairs leads to an asymmetry in plasma density, as demonstrated experimentally here. Modification of the magnetic field topology to enhance its symmetry is currently under development. With the permanent magnets in their designated positions, the value and direction of the filter field current are the free parameters through which the vertical and horizontal homogeneity of plasma density can be optimized, as it is demonstrated in the remainder of this section.

The peculiar behavior of the G1-RFF and G4-SFF – observed in figure 4 – can be attributed to the different behavior of the left and right drivers in these sectors. This is evident when examining the dependency of the ratio of the plasma light measured in the left and right drivers, $I_{\mathrm{PL}}(L)/I_{\mathrm{PL}}(R)$, in each segment, in relation to the filter field (figure 5-panel (*b*)). First, the I_{PL} measured in each pair of drivers tends to exhibit more symmetric (a ratio closer to 1) in the RFF configuration, represented by dashed lines, for all filter current values. The left-to-right ratio of the $\mathrm{I_{PL}}$ in G4-SFF increases as the filter current does; the opposite occurs for the G1-RFF. The effect of the PG and BP bias on the left-to-right ratio is shown in figure 5(*b*) on the right. The only segment in which the ratio worsens when biases are applied is G1-SFF, which can thus explain the decrease in plasma light observed in figure 4. In fact, in the scenario with high biases, when $\mathrm{I_{filter}} \geqslant 1.5$ kA, $I_{\mathrm{PL}}(L)/I_{\mathrm{PL}}(R)$ starts to increase from 1.4 to 1.8. In the RFF configuration, on the other hand, the ratio $I_{\mathrm{PL}}(L)/I_{\mathrm{PL}}(R)$ in G1 remains closer to 1 as the filter field strength increases, improving compared to the low bias scenario. Since it is no possible to power one driver individually (each generator is coupled to two drivers), the tuning of control parameters, which in these cases are the filter field current and the BP and PG biases, is the only way to enhance source performances, particularly in terms of horizontal plasma uniformity. Indeed, as biases are increased, and with a specific filter field current value,

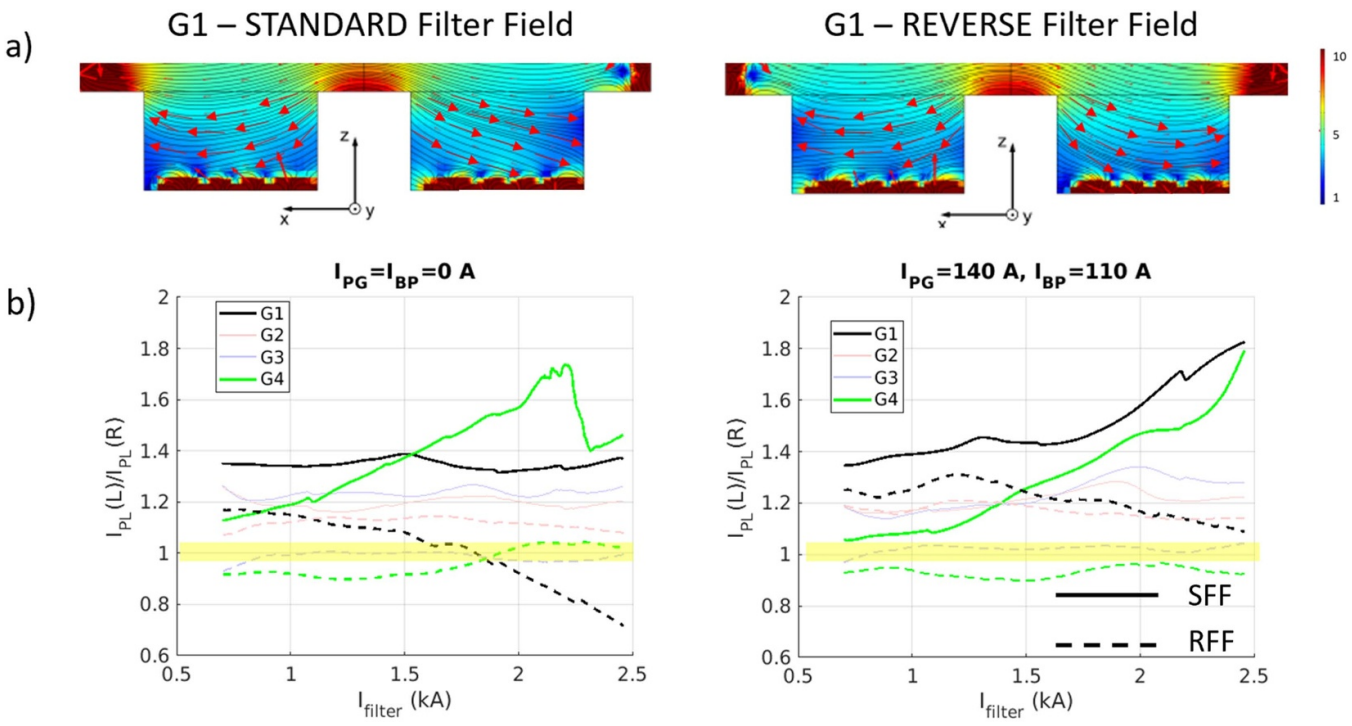

Figure 5. (*a*) Magnetic field distribution with $I_{\text{filter}} = 3$ kA in the SFF (on the left) and RFF (on the right) at the center of the top segment of the source [22]. (*b*) Ratio of the plasma light measured in the left and right drivers in each pair of drivers, as a function of the filter field current for two values of BP and PG biases: $I_{\text{PG}} = I_{\text{BP}} = 0$A on the left, $I_{\text{PG}} = 140\,A$, $I_{\text{BP}} = 110$A on the right. The two line styles represent the two configurations of filter field (solid lines SFF, dashed lines RFF). Reproduced from [22]. CC BY 4.0.

the left to right ratio approaches one, even in the SFF configuration, which is inherently less symmetrical. This analysis underscores that achieving plasma uniformity depends on the filter current (both its direction and magnitude) as well as PG and BP biases. This implies that, in order to obtain uniform plasma, biases have to be adjusted accordingly with the magnetic filter field, to the extent that these adjustments align with the primary function of these controls, namely, the reduction of electron temperature and density in the extraction region.

The vertical uniformity of the plasma density is quantified in figure 6, showing the vertical Root Mean Square (RMS) of the plasma light, defined as

$$RMS = \frac{\sqrt{\sum_{i=1}^{4} \left(I_{\text{PL},i}\,(L+R) - I_{\text{PL,avrg}}\,(L+R)\right)^2}}{I_{\text{PL,avrg}}\,(L+R)}$$

where $I_{\text{PL},i}\,(L+R)$ is the sum of the plasma light measured by the ith pair of drivers and $I_{\text{PL,avrg}}\,(L+R)$ is the average of the sum measured by all four pairs of drivers. On the left is the SFF configuration, on the right is the RFF one.

The minimum RMS, representing the most homogeneous vertical profile of the plasma density, is achieved in the RFF configuration. The specific filter current required for this minimum RMS varies with PG and BP bias. The minimum of the RMS – 15% - is obtained with 1.7 kA of filter current and maximum biases in the RFF configuration. It shifts towards lower filter current values as the biases are reduced, confirming that these two components must be adjusted together to find the optimal working condition. In the SFF configuration, instead, the minimum of RMS is 23%, achieved with 1.35 kA of filter current and maximum biases. It is both larger and at a lower filter current value. For both configurations, increasing the bias of the PG and BP enhances the overall plasma homogeneity. Further increasing the total bias current may be beneficial to enhance plasma homogeneity, although their primary role in reducing co-extracted electrons without worsening beam homogeneity should be considered. However, beyond the point of minimum RMS, further increases in filter current tend to degrade plasma homogeneity. This effect is more pronounced in the RFF configuration, where as the filter field current increases, the RMS approaches (or exceeds) that measured in the SFF, especially when the PG and BP bias is low. On the other hand, for the optimal values of PG and BP bias (represented by the purple series on the right) the RMS remains below 20% for all filter current values.

All these results demonstrate that the optimal configuration for achieving the most homogeneous plasma is the RFF configuration, and both the filter field and biases have an impact on plasma homogeneity in the drivers.

Considering that the minimum RMS corresponds to the case of high biases in both configurations, and therefore higher plasma light (and so plasma density), this suggests that increasing plasma density can enhance the overall plasma homogeneity throughout the source (comparing figures 3, 5(*b*) and 6).

The simplest way to increase plasma density is by raising the RF power.

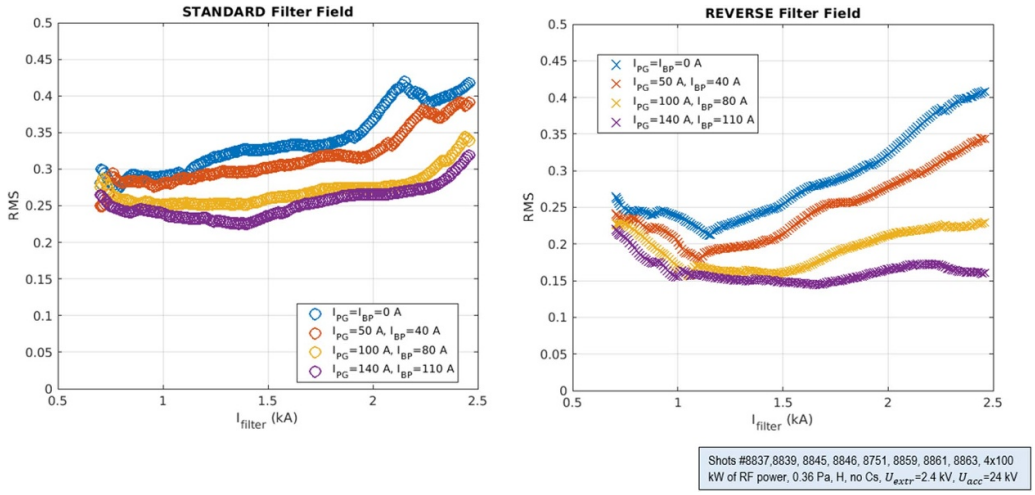

Figure 6. RMS of the total plasma light normalized to the average value as a function of the filter field current in the two configurations – SFF on the left, RFF on the right – for various values of PG and BP bias current.

Figure 7 displays the vertical profile of the sum of plasma light within each pair of drivers (on the left) and its left-to-right ratio (on the right), for various RF power values. The other machine parameters were: 0.4 Pa of H gas, $I_{\text{filter}} =$ 1.5 kA SFF, $I_{\text{PG}} = 80$ A, $\text{I}_{\text{BP}} = 0$ A. The modification of the RMS of the total plasma light is also reported. It is evident that the RMS decreases as the RF power is increased. This increment of the plasma homogeneity can be attributed to the I_{PL} ratio: the asymmetry in the pair of drivers at the bottom of the source (G4-SFF) is significantly reduced as RF power is increased from 60 kW ($I_{\text{PL}}(L)/I_{\text{PL}}(R) =1.92$) to 90 kW ($I_{\text{PL}}(L)/I_{\text{PL}}(R) =1.36$). Although less pronounced, an increase in the left–right symmetry is also observed in the segment at the top of the source.

This provides direct confirmation of the beneficial effect of increasing plasma density to improve plasma homogeneity in the drivers. Therefore, when SPIDER operates at full performance, enhanced homogeneity can be expected.

In the next section, the plasma, after it has expanded in the expansion region, will be examined, and in sections 4 and 5, its connection with the properties of the beam will be investigated.

3. Plasma in the expansion region

The plasma generated in the four pairs of drivers expands towards the extraction region through a magnetic filter field, B_{filter}, which lowers the electron temperature and density to reduce the destruction rate of negative ions.

As shown by numerical simulations in [17] and also measured on SPIDER with the movable LPs [13, 18], in the SFF configuration (current flowing from the top to the bottom of the PG), when a magnetic field is applied a cold and dense plasma flows out from the top part of the driver, while at the bottom, a hot and low-density plasma comes out. The opposite happens when the filter field is reversed [10]. In the filter field, only electrons are magnetized: electron trajectories follow the lines of the magnetic filter field, and electron transport across the field lines is impeded. While ions are free to propagate from the driver, where the plasma is generated, towards the expansion chamber up to the electrodes (z-direction), electron transport along z is strongly affected by B_{filter}.The higher the electron energy, the lower their collisionality, the stronger the reduction of their density due to the filter field. Once the magnetized electrons reach the BP, its positive bias acts as a scrape-off layer for the electrons, creating a flux parallel to the B_{filter}, causing the electron density to decay. A similar effect is induced also by the bias of the PG. There are thus two overlapping conditions: an inhomogeneous plasma generated within the drivers that expands into the expansion zone, where the filter field induces an electron drift, due to the combined effect of the pressure gradient (responsible for the vertical diamagnetic drift) and the electric field, which instead induces a current through the filter (ExB drift). The superimposition of both effects forms the resulting potential of the plasma boundary. This means that, vertically, at some points the electrode (first the BP, then the PG) could be biased at a potential higher than the local plasma potential (thus attracting electrons), while at other points it could attract positive ions if its potential is lower than the local plasma.

Since four pairs of drivers generate the plasma simultaneously in SPIDER, the resulting plasma profile in the expansion region is affected by the different behavior of the various drivers (as investigated in the previous section). SPIDER has both electrostatic [24] and spectroscopic [14] measurements available near the PG and BP. In this section, they are used to characterize the plasma close to the extraction region. In this region, $B_{\text{filter}}(\text{mT}) = 1.67 I_{\text{filter}}(\text{kA})$, and it was experimentally found that less than 1 mT is enough to reduce the electron temperature in front of the BP to a few eV [25]; further increase of the B_{filter} no longer affects the electron temperature.

The H_β plasma emission is used to study the plasma properties in this region. Without a magnetic filter field, H_β emission would be dominated by ionizing processes due to the high

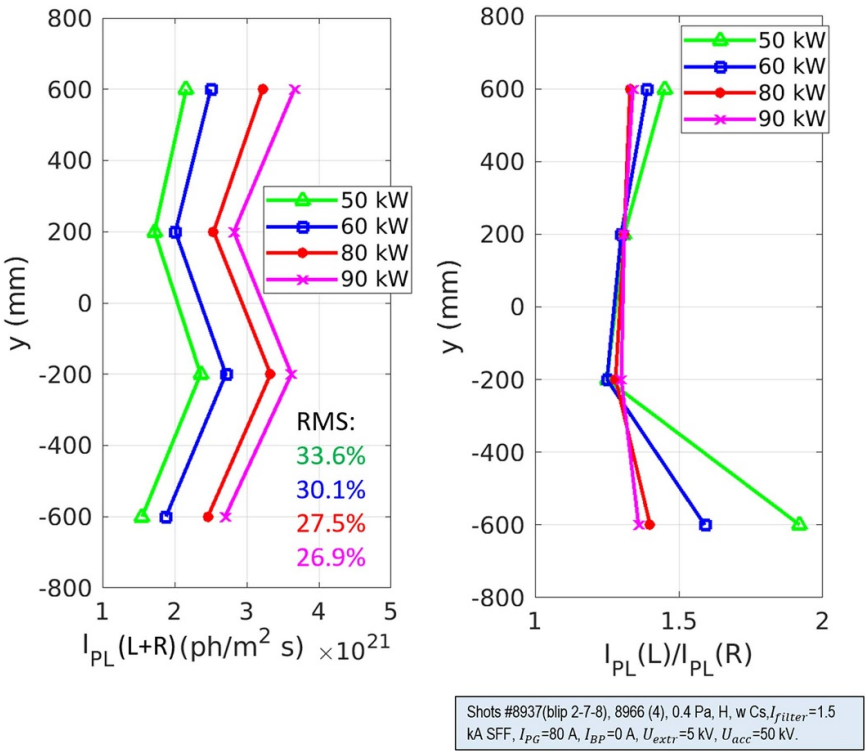

Figure 7. On the left, vertical profile of the sum of the plasma light measured inside each pair of drivers, on the right the ratio between the plasma light measured in the left and right drivers, for various values of RF power.

electron density and temperature, similar to the plasma inside the driver. When the magnetic field is applied, H_β emission is dominated by recombinant processes [15], specifically by the H_2^+ dissociative and mutual (with negative ions) recombination. Therefore, H_β emission is related to electron collisions and heavy particle processes, and not only to the gas dissociation.

A set of windows allows for the measurement of the vertical emission profile of the plasma at a distance of 35 mm from the PG, which is in front of the BP (the upstream surface of the BP is located 20 mm away from the PG, toward the drivers). All lines-of-sight are directed horizontally, meaning they collect the integral of the light emitted by the plasma expanding from both drivers of a given vertical position, collecting one spectrum per second.

Without cesium evaporation (low negative ion density), as the filter field increases the principal contribution to the H_β emission can be attributed to the channel $H_2^+ + e^- \rightarrow H + H(p)$. Unlike what is observed for H_α in the drivers, however, H_β emission depends not only on density but also on the electron temperature. Recombination primarily increases with plasma density but is also sensitive to the reduction of electron temperature. These measurements are compared with the LP measurements. Embedded LP on the BP provide the vertical (and horizontal) profile of positive ion saturation current I_{SAT}^+ measured on the BP itself [26]. During the early operation of SPIDER, these probes were mostly used in saturation mode, providing only the measurement of I_{SAT}^+, which is proportional to $n_e\sqrt{T_e}$. The correlation between these two measurements when the filter field current and the BP and PG biases are varied is shown in figure 8, without cesium evaporation. The I_{SAT}^+ of the probe mounted on the BP is correlated with the H_β emission measured at almost the same vertical position and at 15 mm from the BP. It is important to note that these two diagnostics are not measuring the exact same plasma: the H_β emission is the integrated measurement of the plasma emission along a line-of-sight parallel to the BP, while the LPs locally measure on the BP itself.

Solid marks represent the SFF configuration, while empty ones the RFF configuration; on the left the measurements with $I_{PG} = I_{BP} = 0$ A and on the right with $I_{PG} = 140$ A, $I_{BP} = 110$ A.

Both I_{SAT}^+ and H_β emission measurements decrease when the filter current grows, reflecting the reduction in the plasma density, due to the increasing magnetic filter field. Like the case of H_α emission in figure 4, the highest I_{SAT}^+ and H_β emission are observed in the G1-SFF (solid series) and G4-RFF (empty series), regardless of the applied bias. In the scenario with low biases (the left chart in figure 8) and in the RFF configuration, I_{SAT}^+ and H_β emission decrease with the increase of I_{filter} in a similar manner throughout the entire source, with the lowest measurement in G1-RFF. In the SFF configuration, on the other hand, H_β emission is higher at the bottom and lower at the top, in contrast with the I_{SAT}^+ behavior. This suggests different T_e in the vertical plasma profile in this configuration. H_β emission increases as the electron temperature decreases, in contrast to the behavior of I_{SAT}^+, which decreases with T_e square root. Thus, it can be inferred that there is a higher temperature at the top of the source compared to the bottom in the SFF configuration, and this difference is less pronounced in

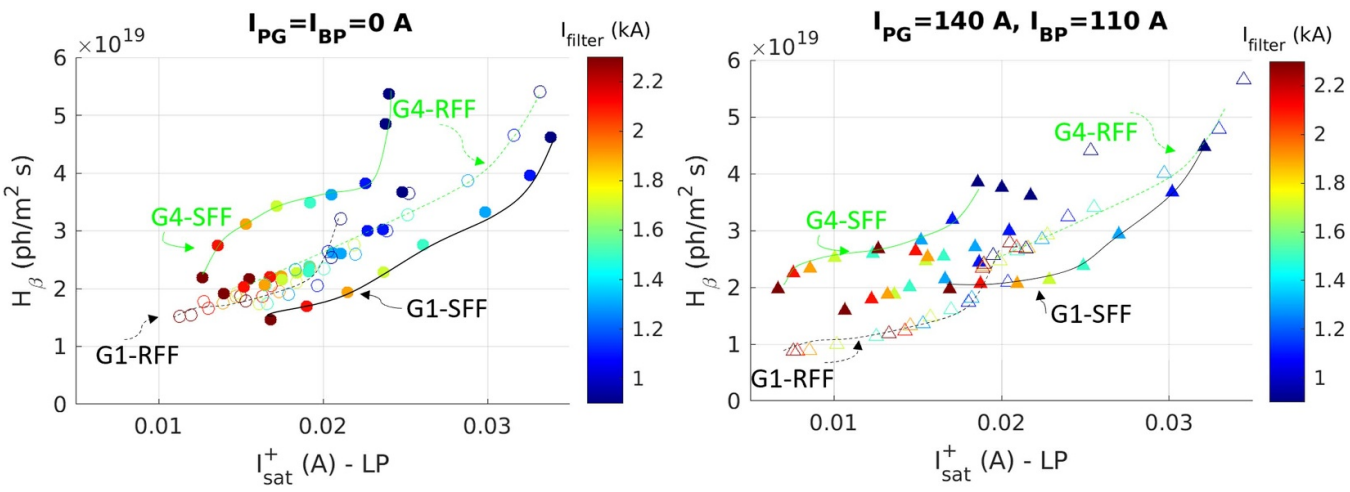

Figure 8. H_β emission measured at 15 mm from the BP, along the lines-of-sight vertically aligned with the driver axis, as a function of the positive ion saturation current measured by the Langmuir probes mounted on the BP, at the same vertical position. Solid marks represent the SFF, empty ones the RFF configuration; on the left the measurements with $I_{PG} = I_{BP} = 0$ A and on the right with $I_{PG} = 140$ A, $I_{BP} = 110$ A.

the RFF configuration (all the points belong to the same line). Additionally, the steep variation of H_β emission for low filter current values in G4-SFF on the right, indicates a change in the processes responsible of this line emission. A similar, though less pronounced, behavior is also observed in G1-RFF (for lower value of filter current).

As the bias of the PG and BP is increased (as shown in the chart on the right of figure 8), the differences between the plasma's vertical profile in both configurations become more pronounced. The minimum of I^+_{SAT} is even lower than the case with low biases, and it is measured in G1-RFF, which also corresponds to the minimum of H_β emission. In contrast, the H_β emission in the G1-SFF decreases as the filter current increases along with the I^+_{SAT}, but after a certain value, it stabilizes while the electrical measurement continues to decrease.

To better visualize the vertical profile of the plasma in this region, the vertical profiles of H_β emission (on the left) and I^+_{SAT} (on the right), both measured with the largest filter current, are shown in figure 9. These profiles represent the two sets of bias conditions for BP and PG: $I_{PG} = I_{BP} = 0$A (in blue) and $I_{PG} = 140$ A, $I_{BP} = 110$ A (in red). Circles and solid lines represent data in the SFF configuration, while triangles and dashed lines represent data in the RFF configuration.

As already observed, when biases increase the vertical H_β profiles become more inhomogeneous, showing larger emissivity at the top with the SFF and at the bottom with the RFF, respectively, than those with zero bias current (blue series). This is also observed in spectroscopic data of similar negative ion sources [25]. Near the grids, the effect of biasing the BP and the PG is obviously stronger than in the drivers. This enhances the top-bottom unbalance of the plasma in the two directions of the filter field. Similar behavior is also measured by the embedded LPs, as shown in the right-hand chart.

Unlike what was observed in the H_β measurements, in the SFF configuration the bias of BP and PG reduces the I^+_{SAT} in the lower part of the source, instead of increasing it in the upper part. Therefore, the final vertical profile of I^+_{SAT} is like that of H_β, but the effect of the bias of these two components is different. In the RFF configuration, however, I^+_{SAT} and H_β have the same behavior. By comparing these two very different measurements - H_β emission and electrical current – it is clear that the effect of the filter field and BP and PG biases is to reduce the total plasma density in front of the grid (the filter field) and to unbalance the vertical plasma profile in this region (the BP and PG biases). The latter also affects the electron temperature. This is predicted by numerical simulations [17, 21] and demonstrated experimentally in other existing negative ion sources [10, 27]. However, this is the first time that the effect of these parameters in a large source as SPIDER is studied. The consequence on the beam behavior are discussed in the following sections, both with and without cesium evaporation in the source.

Another useful piece of information which can be obtained from spectroscopic measurements is the estimation of negative ion density. This is proportional to the ratio of H_α to H_β emissions, in the case of large localized negative ion density, as occurs in surface operation near the PG. The cross sections and rate coefficients are described in detail in [28].

This is shown in figure 10(*a*) for different RF powers (same experimental shots as in figure 7). The H_α/H_β ratio is measured at 5 mm from the PG, during the experimental campaign with cesium evaporation. The cesium acts as a catalyst to produce negative ions, reducing the work function of the grid, which is covered by cesium distributed by the plasma. Full marks represent the line ratio when the beam extraction is active, the empty marks, on the other hand, without beam extraction. The central axis of the drivers is indicated by the dashed black lines, while the cyan lines indicate the extremes of the BP. The change in the line ratio when beam extraction is activated is highlighted by the arrows. Figure 10(*b*) shows the location of the 28 extracted beamlets. By comparing empty (without extraction) and filled (with extraction) green triangles

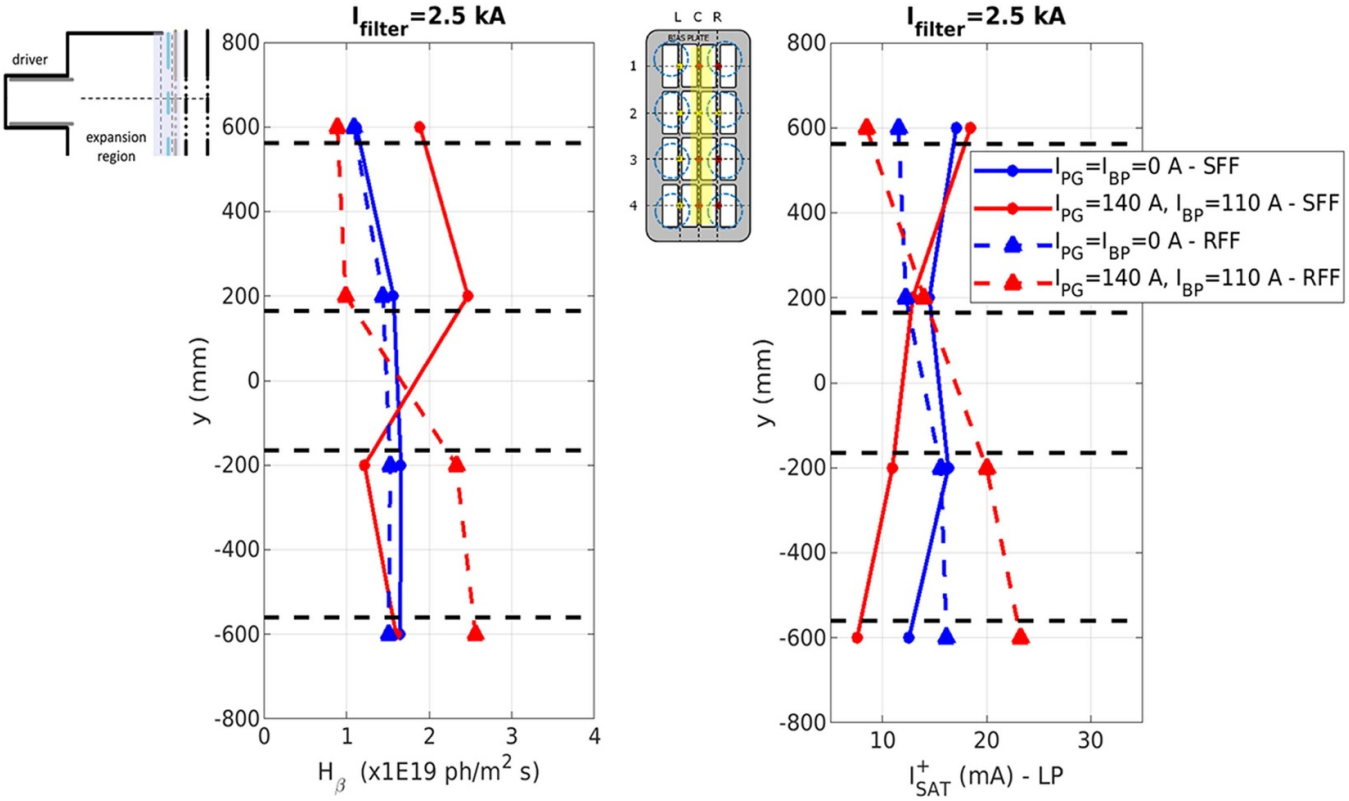

Figure 9. Vertical profile of the H_β emission in front of the BP – on the left – and of the I^+_{SAT} - on the right - in the two directions of the filter field, for the values of BP and PG bias: $I_{PG} = I_{BP} = 0$ A (in blue) and $I_{PG} = 140$ A, $I_{BP} = 110$ A (in red); different marks indicate the diverse directions of the filter field.

the effect of beam extraction on the line ratio can be observed. The line ratio doubles almost everywhere along the vertical beam profile, except in front of the lower driver. Here, the effect of beam extraction on the line ratio for all RF powers is negligible. This can be related to the map of extracted beamlets (figure 10(*b*)). In fact, five beamlets are extracted at that position, while the other lines-of-sight measure the line ratio where only two beamlets are extracted. Negative ions can accumulate near the open apertures where the negative ion density is higher, while the opposite occurs where more beamlets are extracted and the negative ion density is lower, such as at the bottom of the beam. Looking at the green points when there is beam extraction – those at the lowest RF power – it is evident that the negative ion density along the entire vertical profile of the source is non-homogeneous. In fact, if one compares the ratio measured by the central LoS in front of each pair of drivers (i.e. $y = -567$, -165, 165 and 567 mm, indicated by the dashed black lines) one observes a minimum ratio at the bottom of the source. These lines-of-sight are chosen because they are in the same relative position, while the others may be affected by the different distance from the BP components. This may be a direct consequence of the non-uniform vertical plasma density measured inside the drivers and in front of the BP which, consequently, also affects the production of negative ions to be extracted.

Another behavior of the plasma is evinced. As RF power is increased from 50 kW to 60 kW, the negative ion density – the line ratio – increases everywhere along the vertical profile except at the bottom of the source. The further increase to 80 kW, instead, produces no effect on the line ratio, thus suggesting that the negative ions density does not increase proportionally. This can be explained by the non-optimal cesium coverage of the PG. This is also confirmed by the analysis of the vertical profile of the beam, which is discussed in the following section. Since the physics of negative ion beam without and with cesium evaporation in the source is quite different, the beam properties in these two regimes are studied separately.

4. Beam in volume operation

The formation of H^- negative ions in low-pressure hydrogen discharges is primarily due to the dissociative electron attachment to vibrational excited molecules [29]. For this reason, high molecular and electron densities are desirable.

In volume production, negative ions are generated with equal probability throughout the plasma volume, from the driver to the extraction region, proportionally to the plasma density, without spatial preferences.

Once generated within the drivers, the plasma drifts to the expansion region, where the filter field reduces the electron temperature, and, along with the PG and BP bias, decreases its density, thereby reducing the probability of negative ions being destroyed. These parameters act uniformly along the

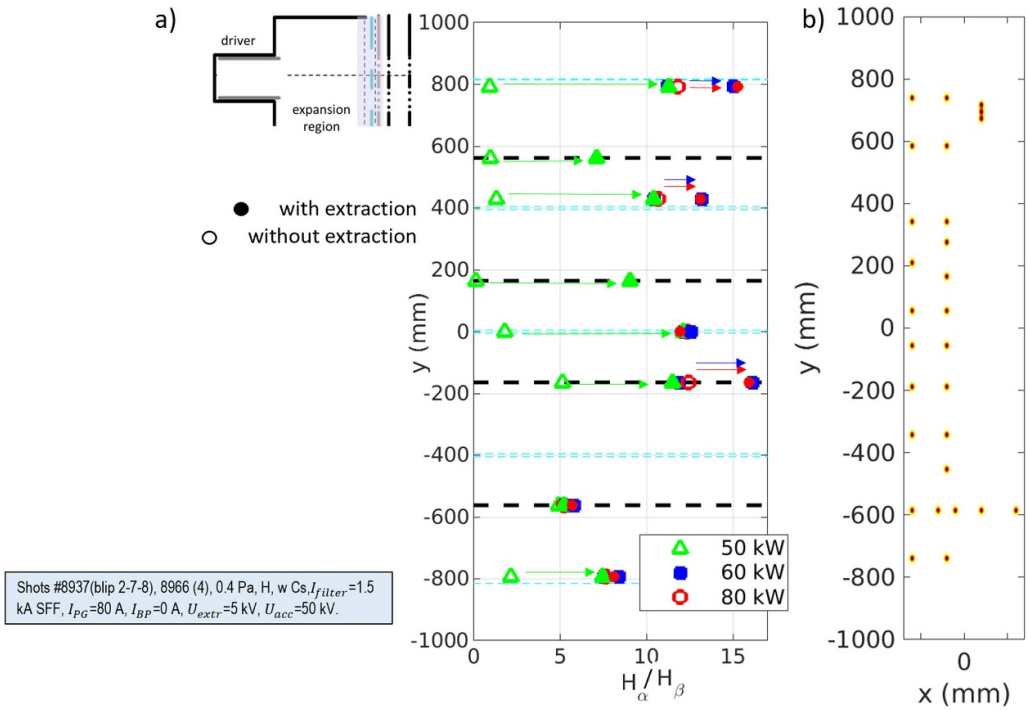

Figure 10. (*a*) Vertical profile of H_α/H_β in front of the PG, as a function of the RF power applied to each pair of drivers (SFF configuration). Empty and full marks represent the measurement without and with beam extraction, respectively. The arrows highlight the change in the line ratio without and with extraction. (*b*) Map of the 28 open beamlets.

entire vertical extent of the plasma. For this reason, the plasma density within the drivers can be used as an indicator of the likelihood of negative ions to be generated along the vertical plasma profile, upon which other machine parameters act as the plasma approaches the extraction zone. The main effect of the PG and BP biases on the plasma has been discussed in the previous sections. By reducing the plasma density, they also decrease the amount of co-extracted electrons. As an estimate of the co-extracted electron current, the current measured by the power supply of the extraction grid is used. In fact, electrons are deflected onto the extraction grid by the permanent magnets installed within the grid itself, so it can be assumed that the measured current consists only of electrons. Due to their larger mass, negative ions are not dumped on the extraction grid by the magnetic field, and they constitute the main contribution to the current measured by the acceleration power supply. The effect of the filter field and the total bias current on both the co-extracted electron-to-ion ratio $(I_\mathrm{e}/I_\mathrm{beam})$ and total beam emissivity, defined as the sum of the tomographically reconstructed emissivity of the 28 open beamlets, which is directly proportional to the beam current density [30], is shown in figure 11. These data were taken under conditions like those just discussed: 0.36 Pa of source pressure, in hydrogen, 4 × 100 kW of RF power, and three values of filter field current $I_\mathrm{filter} = 0.75$, 1.2 and 1.8 kA. The total bias current of the BP and the PG is increased from zero to 110 A and from zero to 140 A, respectively. The same pulses are repeated in the two directions of magnetic filter field. The ratio between the extraction and the acceleration voltages is fixed to 10, with $U_\mathrm{extr} = 2.4$ kV and $U_\mathrm{acc} = 24$ kV, which corresponds to the optimum ratio for the beam optics in volume operation [31]. Typical value of beam current density achieved in volume operation is about 50 $\frac{A}{m^2}$ [8].

The different colors represent various values of filter field current, while the markers indicate the direction of the current flowing onto the PG (full circles for the SFF, crosses for the RFF). As expected, the higher the filter field, the lower the co-extracted electron-to-ion current ratio, which decreases by 65%–70% when the filter current is varied from 0.75 to 1.8 kA. A slight dependence of $\frac{I_e}{I_{beam}}$ on the filter field direction is evinced for all the values of filter current: the ratio is lower in the RFF configuration. The $\frac{I_e}{I_{beam}}$ decreases also when the total bias current grows, reducing from 14 to 8 for the high filter case (1.8 kA). In all studied configurations (various filter field currents in the two directions), the negative ion current (here represented by the total beam emissivity measured by visible tomography – right panel of figure 11) is almost independent on the total bias current of the BP and PG. In the RFF at least 20% higher emissivity and a lower electron-to-ion current ratio than in SFF are detected. The fact that the optimal value of filter current – in terms of beam current performance – is an intermediate value is a consequence of what observed in the drivers and expansion region. A too strong filter field, although beneficial for the plasma in the drivers, excessively reduces the plasma density in the expansion region, thereby also reducing the negative ion density.

These measurements give information regarding the collective behavior of SPIDER beam when the filter field strength and the BP and PG biases are varied. Beam tomographic reconstruction also allows studying how they affect the beam

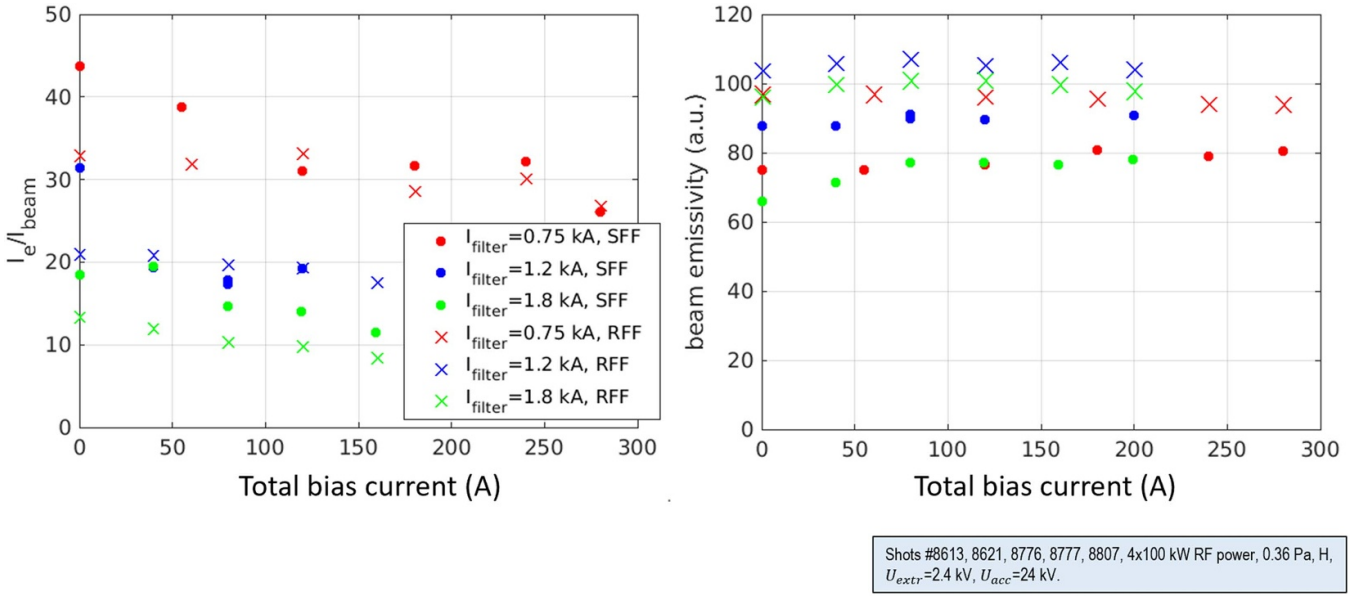

Figure 11. I_e/I_{beam} (on the left) and total beam emissivity (on the right) as a function of the sum of the total bias current, for diverse values and directions of the filter field.

locally [30]. The beam 2D pattern is characterized using the beamlet emissivity reconstructed through the tomographic inversion, with one value for each of the 28 extracted beamlets. In this way, the vertical profile, as well as the dynamics inside each beamlet group can be studied.

A direct comparison between the beam vertical profile in the two configurations of filter field, for two values of total bias currents is shown in figure 12. To study the vertical profile of the beam, only beamlets belonging to the leftmost column are used, to compare beamlets with the same position with respect to the center of (right) drivers, as highlighted in the red inset on the left of figure 12. As already suggested by Figure 11(right), the reconstructed total beam emissivity is overall larger in the RFF configuration. The difference between SFF and RFF tendentially increases from top to bottom. This behavior could be compared with the plasma light data shown in figure 4, both in terms of inversion of the filter field direction and bias currents. In the SFF configuration, in fact, I_{PL} (tot) is higher at the top and lower at the bottom of the source, where it increases with biases. In the RFF configuration, on the other hand, I_{PL} (tot) increases with biases at the top of the source. The same relative change is observed in the emissivity of the beam: at the bottom, when the biases increase, the emissivity of the beam also increases. In RFF the opposite happens: the only change in beam emissivity, as biases are increased, is measured at the top of the beam. In volume operation this could be explained in terms of plasma density growth and, thus, of the probability of negative ions to be produced. Since the plasma density in the SFF (RFF) is lower at the bottom (at the top) of the source, the effectiveness of the BP and PG bias is stronger especially in this region; this explains the observed change in beam emissivity and demonstrates the close connection between beam and plasma properties.

5. Beam in surface operation

In surface production, the negative ions are generated when hydrogen (or deuterium) atoms bounce off walls coated with cesium, which with its low work function is exploited as a source of electrons. Experimentally, when a small amount of Cs vapor is evaporated into the source, a fast decrease of the co-extracted electron current occurs, accompanied by a growth of the negative ion current [32]. In SPIDER, beam current density up to 200 $\mathrm{A\,m^{-2}}$ is achieved, with 100 kW per RF generator [8]. In this negative ion production regime, the plasma in front of the PG plays a fundamental role since this is the region where most of the negative ions are produced and then extracted.

Spectroscopic measurements in figure 7 show that the plasma density depends on the applied RF power, thus influencing the density of negative ions available for extraction, and therefore the shape of the meniscus, which is the region between the negative ion beamlet and the neutral plasma.

The increase of the total current, in terms of the beam emissivity, as the RF power is increased is shown in figure 13 – blue marks. In analogy to the negative ion density in the source (line ratio in figure 10), the largest increase in the total beam current occurs between 50 and 60 kW – and amounts to around 25%. Then, as the power is further increased, the total beam current – as the negative ion density – exhibits a lower slope. The increase of the total beam current results in a modification of the beam homogeneity. In this work, beam homogeneity is quantified using as a figure of merit the average RMS divided by the mean value of total emissivity: $\frac{RMS}{\text{avrg}} = \sqrt{\frac{\sum_{i=1}^{n_{\text{beamlet}}} (\in_i - \in_{\text{avrg}})^2}{n_{\text{beamlet}}}} / \in_{\text{avrg}}$, where n_{beamlet} is the total number of beamlets whose homogeneity is studied, $\in_{\text{avrg}}$ is the mean value of the reconstructed emissivity and $\in_i$ the emissivity of

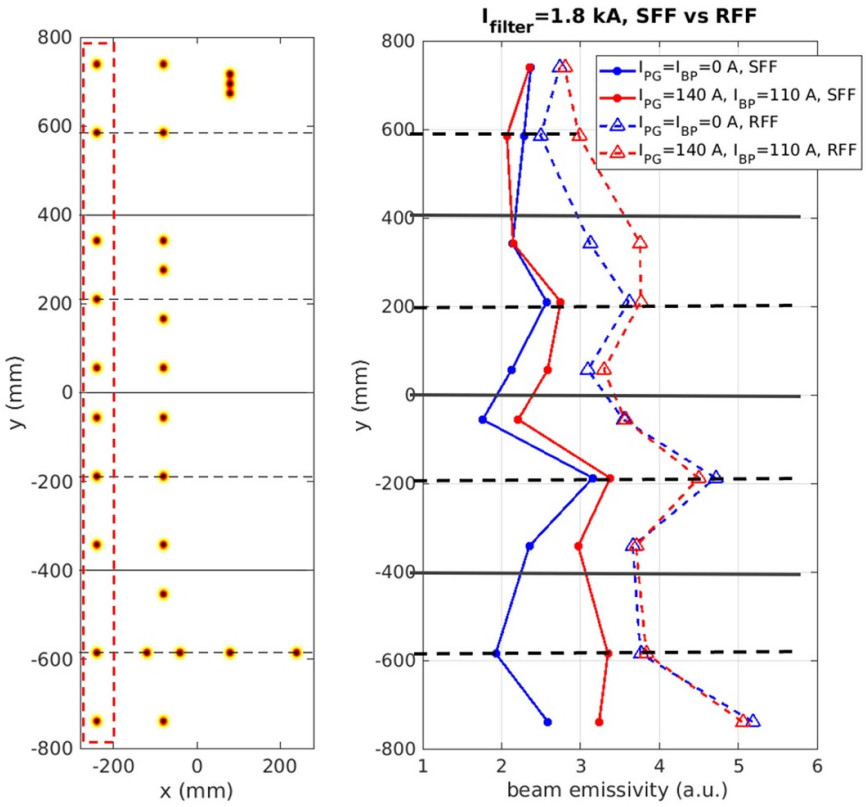

Figure 12. Vertical profiles of the beam emissivity of the external column of open beamlets (highlighted in red in the scheme on the left) as a function of the total bias current of the BP and PG, in the two directions of filter field.

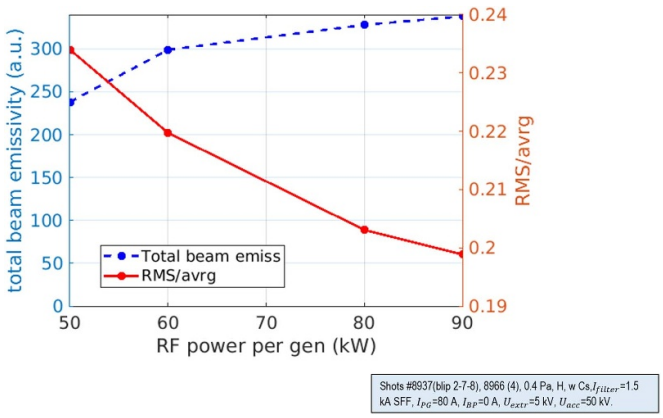

Figure 13. RMS/average (in red-solid line) and total beam emissivity (in blue-dashed line) as a function of the RF power per generator.

the *i*th beamlet. The normalized RMS of the beamlet emissivity is shown in figure 13 – red points. The normalized RMS decreases as the RF power grows, up to a minimum of 20%.

To better understand how the beam current is modified with the RF power along the entire beam vertical profile, the vertical profiles of the beam emissivity for the four different values of RF power are shown in figure 14(*a*). Each point represents the reconstructed emissivity of each beamlet composing the external column of open beamlets (see scheme in figure 12). The correspondent vertical profiles of the beamlet width are shown in figure 14(*b*). The beamlet width is the 1/*e* width given by the 1D Gaussian fit of the single beamlet profile, measured by different visible-range cameras observing the beam.

As the RF power increases, the emissivity of the beamlets grows non-homogeneously along the vertical profile. The beamlet with the lowest emissivity is the one at the bottom of the beam. Furthermore, beamlets at the bottom of each beamlet group have a lower emissivity than those at the center and top of the same group. They are also more sensitive to modification of the RF power, as confirmed by the wider variation of their widths, which decrease as the RF power grows. Central beamlets of each beamlet group have a similar width and emissivity, except for the lowest value of RF power, as already observed in figure 10.

This different vertical behavior of the beam can be explained by the non-homogeneous negative ion density along the beam vertical profile. In fact, when the RF power is low, not enough negative ions are available for beamlets at the bottom to be extracted, thus their divergence is larger (too concave meniscus) with respect to the other beamlets; as the plasma density increases their optics improves, confirming the larger negative ion density. This affects especially the beamlets at the extreme of beamlet groups, which are the regions sensitive the most to the overall increase of the plasma density (in this case, due to the RF power).

The horizontal beam homogeneity can be studied at the bottom of the beam, where five beamlets belonging to the same row are extracted, as shown in figure 14(*d*): there, in fact,

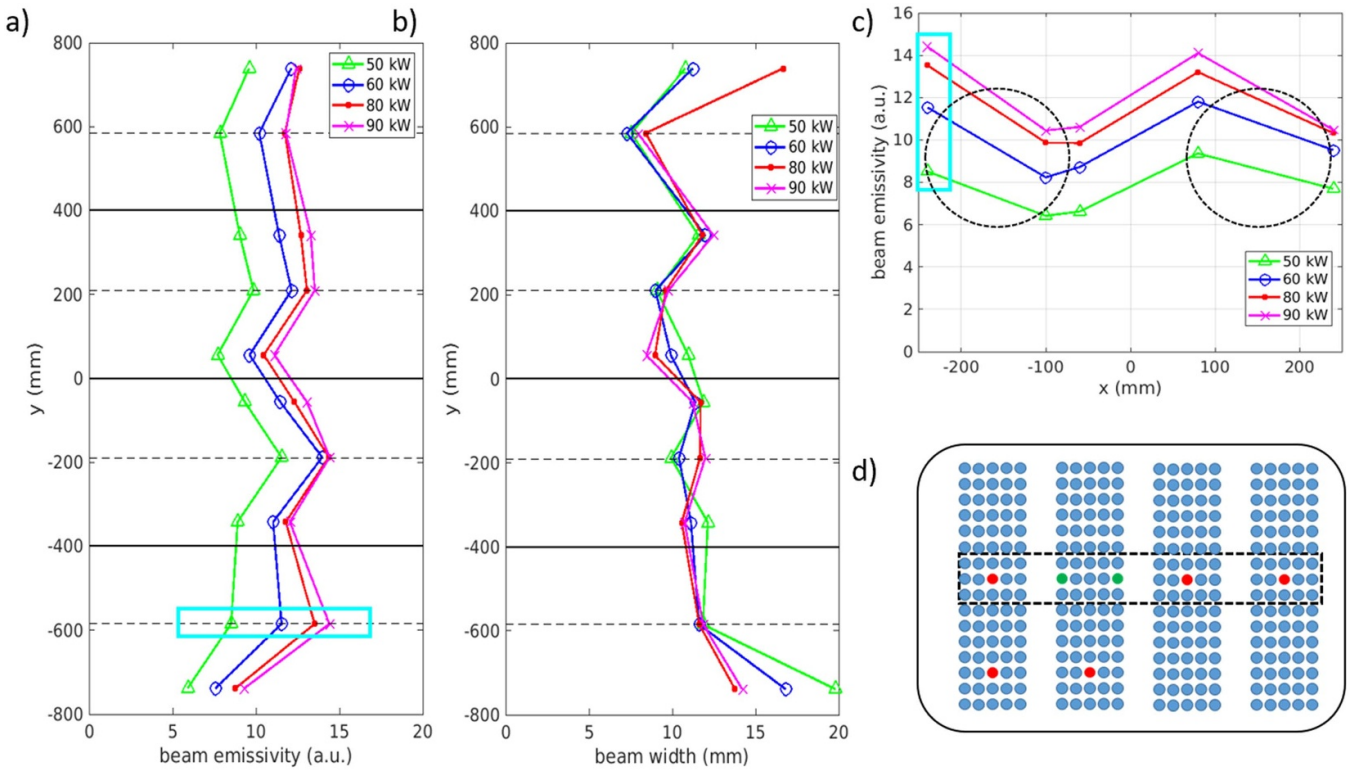

Figure 14. Vertical profile (external column) of beam emissivity (*a*) and width (*b*) as a function of the RF power. (*c*) Horizontal profile of the beam emissivity of the beamlets at the bottom of the source (schematic representation in (*d*)), as a function of the RF power.

five beamlets are extracted distributed among both drivers. As shown in figures 3 and 5, a different plasma density is measured inside the two drivers at the bottom of the source, especially in the SFF filter configuration. This partially affects also the beamlet current density, as shown in figure 14(*c*). The two beamlets at the exact same position with respect to the drivers are the external beamlets ($x = -240, +240$). The lower plasma density of the left driver with respect to the right one (see figure 5) results in a lower beam current density for the leftmost beamlet. Furthermore, a lower beamlet emissivity is also measured for the beamlets at the extreme edges of a beamlet group, indicated in green in figure 14(*d*).

All measurements shown above demonstrate that the vertical beam current density profile is non-homogeneous, reflecting the non-uniformity of the plasma both inside the drivers and close to the grids. To show how strongly this is related to a non-homogeneous plasma vertical profile, the RF power delivered by the four generators is adjusted, trying to compensate the lower negative ion density by increasing the RF power of the generator at the bottom with respect to the others (in the SFF configuration). This also demonstrates that drivers essentially act on the plasma - and thus on the part of the beam - in front of them.

The vertical profile of the total plasma light measured inside each pair of drivers, the H_β emission in front of the BP, the beam emissivity and divergence of the external column of beamlets are shown, respectively, in figures 15(*a*)–(*d*); in blue the measurements with all generators supplying the same power, in red with adjusted RF power. From the top to the bottom of the plasma source, the applied power in the adjusted configuration is 45-65-55-80 kW per generator.

The effect of such unbalancing is evident in all the measurements, highlighting again also the connection between the plasma and the beam properties. As the RF power is adjusted, both the total plasma light in the drivers and the H_β emission in front of the BP at the bottom of the source increase, as evidence of the plasma density growth in this region. This affects both the vertical beam emissivity and width, resulting in a more homogeneous profile and in a decrease of the width especially at the bottom of the beam, due to the increase in the extracted negative ion current. Even if this is just a preliminary result and it was tested only at low power, it demonstrates how it is possible to obtain a more homogeneous beam, in the operational regime explored up to now. It is not straightforward that this will be repeatable also at higher power, but if it is related to an unbalancing in the total drift of the plasma, in opposition to the drift due to the filter field (here in SFF configuration), it could work also with higher power.

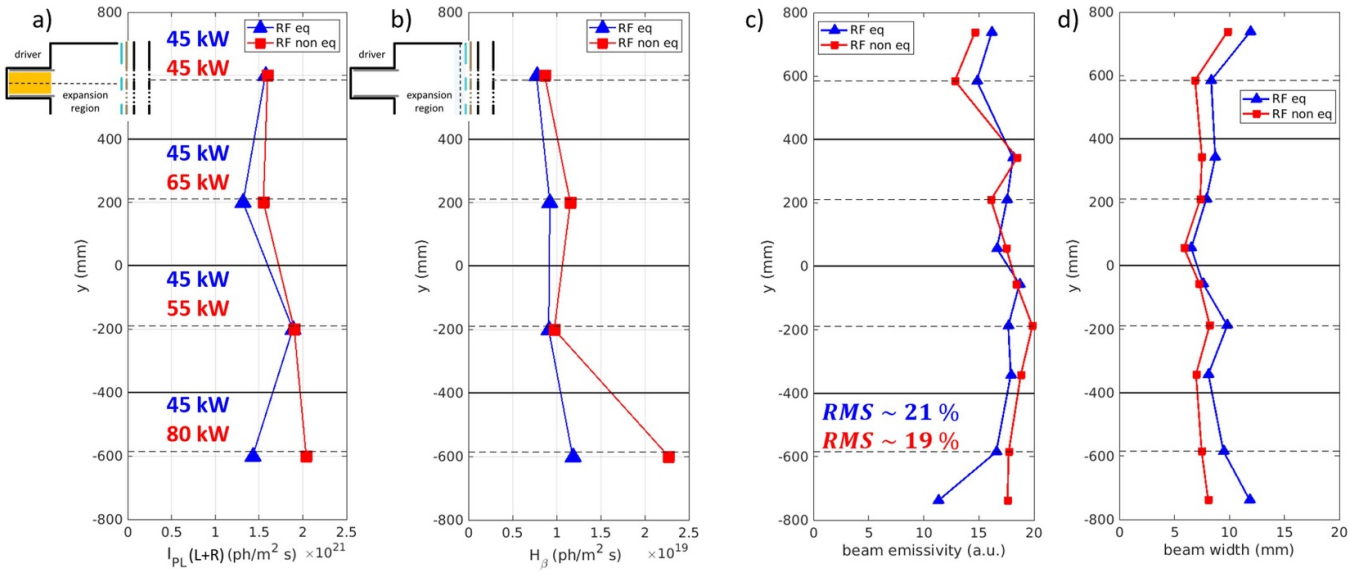

Figure 15. Vertical profile of the total plasma light measured inside each pair of drivers (*a*), the H_β emission in front of the BP (*b*), the beam emissivity (*c*) and divergence (*d*) of the external column of beamlets; in blue the measurements with all generators supplying the same power, in red with adjusted radio-frequency power.

6. Summary

In this paper, the properties of the plasma, from the drivers to the extraction region throughout the expansion region, are studied starting from the information given by spectroscopic and electrostatic measurements and related with the beam features studied through visible tomography.

- The H_α emission inside each RF driver is correlated with the electron density measured by LPs inserted inside the driver, during a dedicated experimental campaign. Once demonstrated that those measurements are linearly dependent, H_α emission is used as an estimate of the plasma density in the drivers along the entire vertical profile of the source. The plasma produced inside each driver is characterized, focusing on the key role played by the plasma density, when the main machine parameters are varied, such as the RF power, the filter field strength and direction and the bias of the BP and PG.
- A lower plasma density is measured in the drivers at the bottom of the source in the standard direction of the filter field, at the top in the reversed one, for all values of filter current experimentally explored. However, this top-to-bottom non-uniformity does not reverse perfectly when the filter field is reversed, indicating that it is not solely dependent on this parameter. One possible explanation can certainly be attributed to the inherent structure of the source, which is composed of 4 independent generators that couple with the plasma in pairs of horizontal drivers. Further insight was provided by examining the left–right symmetry of these pairs of drivers.
- As the filter field is increased, the plasma light measured in the drivers grows, but it acts differently on the various pairs of drivers. In fact, when the filter current is increased, the difference between the plasma density of the two drivers at the bottom in the SFF, at the top in the RFF, respectively, grows, resulting in an increasing of left-to-right asymmetry. From the analysis of plasma emission, another peculiar behavior is found inside the SPIDER source: when the filter field is reversed, the difference between the plasma light measured in these pairs of drivers is reduced, resulting in a denser plasma with the same RF power and source pressure. This behavior is explained by examining the magnetic field profile within the upper drivers of the source. In fact, when the filter field is reversed, its topology within the drivers becomes more symmetrical, allowing for a more symmetric plasma to be achieved.
- By varying both the filter field and the bias of the PG and BP within the maximum experimental range, the plasma homogeneity is studied. This is assessed through the RMS of the plasma light emitted by the eight drivers that compose the source. The minimum RMS varies with changes in these parameters, demonstrating the need to set them appropriately to optimize the source's operation within the bounds of correct functionality and to enhance beam performance, which is their primary purpose.
- The dependence of the plasma homogeneity on the plasma density is experimentally demonstrated by varying the RF power, which is the primary tool for increasing plasma density, showing that plasma homogeneity increases with higher plasma density.
- The plasma profile is then studied close to the PG, where the negative ions are mostly produced (during the operation with cesium evaporation) and then extracted. Due to the low temperature of the plasma in this region, because of the effect of the magnetic filter field, the plasma in this region is completely different from the ionizing plasma in the drivers. Recombinant processes play fundamental role in the plasma emission. The H_β emission is compared with the positive ion saturation current measured by the LPs. Both

these measurements are sensitive not only to the plasma density, but also to the variation of the electron temperature. They both show how the plasma in this region is strongly affected by the modification of both the filter field and the bias of the PG and BP. The latter increases the inhomogeneity of the plasma, affecting the most the region where the plasma is less dense, i.e. at the bottom in the SFF, at the top in the RFF. This has demonstrated that, although plasma drifts resulting from the filter magnetic field, combined with the bias of the PG and BP, induce a complex vertical dynamic within the plasma in this region, the plasma in front of the PG is still significantly influenced by the plasma in the drivers from which it originated, even though all the plasma mixes as it drifts within the expansion region.

The vertical profile of the plasma is then compared with the one of the beam, correlating the behavior of the plasma with the properties of the beam. The beam emissivity reconstructed through tomographic inversion is used as an estimate of the single beamlet current density, both without and with cesium evaporation.

- The increase of the PG and BP bias slightly reduces the beam top-bottom non-homogeneity in volume operation, by increasing the beamlet current density at the bottom of the beam in the standard direction, at the top in the reverse direction of the filter field. This was also observed in terms of plasma density inside the drivers, which enhances with the biases respectively at the bottom and at the top of the source, in the two configurations. The local increase of the beam current density can thus be related to the larger plasma density and, consequently, a higher probability of negative ion production in the whole plasma volume in front of those drivers.
- To study the dependence of the beam current density vertical profile on the plasma density, the beam homogeneity is studied when the RF power is increased. As confirmed by the H_α/H_β line ratio, the negative ion density is non-uniform along the vertical profile of the beam, with a minimum at the bottom. When the RF power is increased, the higher plasma density translates into a more homogeneous beam, with an increase in current density at the bottom in the standard filter configuration, precisely where plasma density is usually lower. This is a confirmation of the beneficial effect of having a denser plasma, in order to have enough negative ions to be extracted along the entire vertical profile of the beam.
- As a further confirmation of that, once demonstrated the unbalance of the vertical plasma density, the RF power was adjusted accordingly to make the vertical plasma density profile more uniform among the four pairs of drivers comprising the source. As a consequence of that, the beam vertical profile becomes more homogeneous when a larger RF power is applied to the drivers at the bottom with respect to the ones at the top, in the SFF configuration. This method works for RF power comprised between 45 and 80 kW per generator. Further experiments must be carried out at larger RF power, to see if this solution is applicable also to higher RF power regimes.

7. Conclusions

In this paper the strict connection between the plasma density and the homogeneity of both the plasma in the source and the beam is demonstrated, using spectroscopic and electrostatic measurements. The relationship between the plasma density and the filter field direction and intensity, as well as the bias of the PG and BP, is analyzed when these parameters are varied.

We have defined the parameter space where both the plasma density and homogeneity are optimal.

Also, the homogeneity of plasma in the source depends on the direction of the filter field.

The plasma density is increased in absolute value, by increasing the total RF power, and in relative, by increasing the RF power only in the drivers where the lowest plasma density is measured. In both cases, the beam homogeneity improved, resulting in a more homogeneous distribution of the current along the vertical profile and, consequently, in a lower – in the regions where the plasma density grows - and more homogeneous beam divergence.

All these results suggest that one solution to improve the performance of this large-size negative ion source is to increase the plasma density. Adjusting the RF power, in fact, although proved satisfactory in increasing beam homogeneity, means operating with lower RF power for some generators, which may not be a solution to meet the requirements of ITER HNBs.

One potential solution to enhance plasma density is to improve the confinement of the plasma itself, a development currently underway in SPIDER.

Acknowledgments

This work has been carried out within the framework of the ITER-RFX Neutral Beam Testing Facility (NBTF) Agreement and has received funding from the ITER Organization. The views and opinions expressed herein do not necessarily reflect those of the ITER Organization. This work has been carried out within the framework of the EUROfusion Consortium, funded by the European Union via the Euratom Research and Training Programme (Grant Agreement No. 101052200—EUROfusion). Views and opinions expressed are however those of the author(s) only and do not necessarily reflect those of the European Union or the European Commission.

ORCID iDs

M. Ugoletti https://orcid.org/0000-0002-7498-0780
M. Agostini https://orcid.org/0000-0002-3823-1002
C. Poggi https://orcid.org/0000-0001-8482-803X
E. Sartori https://orcid.org/0000-0002-5651-1825
G. Serianni https://orcid.org/0000-0002-4704-2019
B. Zaniol https://orcid.org/0000-0001-9934-8370

References

[1] Agostinetti P. *et al* 2011 Physics and engineering design of the accelerator and electron dump for SPIDER *Nucl. Fusion* **51** 063004

[2] Marcuzzi D., Agostinetti P., Dalla Palma M., Degli Agostini F., Pavei M., Rizzolo A., Tollin M. and Trevisan L. 2010 Detail design of the beam source for the SPIDER experiment *Fusion Eng. Des.* **85** 1792–7

[3] Pavei M. *et al* 2020 SPIDER plasma grid masking for reducing gas conductance and pressure in the vacuum vessel *Fusion Eng. Des.* **161** 112036

[4] Sartori E. *et al* 2022 First operations with caesium of the negative ion source SPIDER *Nucl. Fusion* **62** 086022

[5] Serianni G. *et al* 2022 Spatially resolved diagnostics for optimization of large ion beam sources *Rev. Sci. Instrum.* **93** 081101

[6] Heinemann B., Fantz U., Kraus W., Schiesko L., Wimmer C., Wünderlich D., Bonomo F., Fröschle M., Nocentini R. and Riedl R. 2017 Towards large and powerful radio frequency driven negative ion sources for fusion *New J. Phys.* **19** 015001

[7] Marconato N., Brombin M., Pavei M., Tollin M., Baseggio L., Fincato M., Franchin L., Maistrello A. and Serianni G. 2021 An optimized and flexible configuration for the magnetic filter in the SPIDER experiment *Fusion Eng. Des.* **166** 112281

[8] Serianni G. *et al* 2023 SPIDER, the negative ion source prototype for ITER: overview of operations and cesium injection *IEEE Trans. Plasma Sci.* **51** 1–9

[9] Wimmer C. *et al* 2018 Influence of external magnets and the potential rods on the plasma symmetry in the ELISE ion source *AIP Conf. Proc.* **2052** 040003

[10] Schiesko L., McNeely P., Franzen P. and Fantz U. 2011 Magnetic field dependence of the plasma properties in a negative hydrogen ion source for fusion *Plasma Phys. Control. Fusion* **54** 105002

[11] Tsumori K. and Wada M. 2017 Diagnostics tools and methods for negative ion source plasmas, a review *New J. Phys.* **19** 045002

[12] Pasqualotto R., Barbisan M., Lotto L., Zaniol B., Bernardi M. and Franchin L. 2019 Plasma light detection in the SPIDER beam sourc *Fusion Eng. Des.* **146** 709–13

[13] Sartori E. *et al* 2021 Development of a set of movable electrostatic probes to characterize the plasma in the ITER neutral beam negative-ion source prototype *Fusion Eng. Des.* **169** 112424

[14] Zaniol B., Barbisan M., Bruno D., Pasqualotto R., Taliercio C. and Ugoletti M. 2020 First measurements of optical emission spectroscopy on SPIDER negative ion source *Rev. Sci. Instrum.* **91** 013103

[15] Wunderlich D., Giacomin M., Ritz R. and Fantz U. 2019 Yacora on the web: online collisional radiative models for plasmas containing H, H2 or He *J. Quant. Spectrosc. Radiat. Transfer* **240** 106695

[16] Boef J.P., Chaudhury B. and Garrigues L. 2012 Physics of a magnetic filter for negative ion sources. I. Collisional transport across the filter in an ideal, 1D filter *Phys. Plasmas* **19** 113509

[17] Lishev S., Schiesko L., Wünderlich D., Wimmer C. and Fantz U. 2018 Fluid-model analysis on discharge structuring in the RF-driven prototype ion-source for ITER NBI *Plasma Sources Sci. Technol.* **27** 125008

[18] Poggi C. Numerical and experimental study of the physics of Negative ion beams *PhD Thesis*

[19] Casagrande R. *et al* 2022 Techniques to widen the operational space of SPIDER radio frequency driven plasma source *J. Phys.: Conf. Ser.* **2244** 012054

[20] Maistrello A. *et al* 2023 Overview on electrical issues faced during the SPIDER experimental campaigns *Fusion Eng. Des.* **190** 113510

[21] Fubiani G. and Boeuf J.P. 2015 Three-dimensional modeling of a negative ion source with a magnetic filter: impact of biasing the plasma electrode on the plasma asymmetry *Plasma Sources Sci. Technol.* **24** 055001

[22] Marconato N., Sartori E. and Serianni G. 2022 Numerical and experimental assessment of the new magnetic field configuration in SPIDER *IEEE Trans. Plasma Sci.* **50** 3884–9

[23] Sartori E. *et al* 2023 Highlights of recent SPIDER results and improvements *J. Instrum.* **18** C09001

[24] Spolaore M., Serianni G., Leorato A. and Agostini F.D. 2010 Design of a system of electrostatic probes for the RF negative ion source of the SPIDER experiment *J. Phys. D: Appl. Phys.* **43** 124018

[25] Fantz U. *et al* 2021 Negative hydrogen ion sources for fusion: from plasma generation to beam properties *Front. Phys.* **9** 709651

[26] Poggi C. *et al* 2022 Langmuir probes as a tool to investigate plasma uniformity in a large negative ion source *IEEE Trans. Plasma Sci.* **50** 3890–6

[27] Kisaki M. *et al* 2012 Electron density measurement of cesium seeded negative ion source by surface wave probe *Rev. Sci. Instrum.* **83** 02B113

[28] Fantz U., Falter H., Franzen P., Wünderlich D., Berger M., Lorenz A., Kraus W., McNeely P., Riedl R. and Speth E. 2006 Spectroscopy a powerful diagnostic tool in source development *Nucl. Fusion* **46** S297–306

[29] Bacal M. 2006 Physics aspects of negative ion sources *Nucl. Fusion* **46** S250

[30] Ugoletti M., Agostini M., Pimazzoni A., Sartori E. and Serianni G. 2022 SPIDER beam homogeneity characterization through visible cameras *IEEE Trans. Plasma Sci.* **50** 3913–21

[31] Pimazzoni A., Brombin M., Canocchi G., Delogu R.S., Fasolo D., Franchin L., Laterza B., Pasqualotto R., Serianni G. and Tollin M. 2020 Assessment of the SPIDER beam features by diagnostic calorimetry and thermography *Rev. Sci. Instrum.* **91** 033301

[32] Bacal M., Michaut C., Elizarov L.I. and El Balghiti F. 1996 Basic processes of negative hydrogen ion production and destruction in sources and beams *Rev. Sci. Instrum.* **67** 1138